First-principles study of Ti-doped sapphire. II. Formation and reduction of complex defects

Weiguo Jing,[1,2,3] Mingzhe Liu,[1,4] Jun Wen,[5] Lixin Ning,[6] Min Yin,[4] and Chang-Kui Duan[1,2,3,*]

[1]*Hefei National Laboratory for Physical Sciences at the Microscale and Department of Physics, University of Science and Technology of China, Hefei 230026, China*

[2]*CAS Key Laboratory of Microscale Magnetic Resonance, University of Science and Technology of China, Hefei 230026, China*

[3]*CAS Center for Excellence in Quantum Information and Quantum Physics, University of Science and Technology of China, Hefei 230026, China*

[4]*CAS Key Laboratory of Strongly-Coupled Quantum Matter Physics, University of Science and Technology of China, Hefei 230026, China*

[5]*School of Electronic Engineering and Intelligent Manufacturing, Anqing Normal University, Anqing 246133, China*

[6]*Anhui Province Key Laboratory of Optoelectric Materials Science and Technology, Key Laboratory of Functional Molecular Solids, Ministry of Education, Anhui Normal University, Wuhu, Anhui 241000, China*

(Received 6 July 2021; revised 19 September 2021; accepted 21 September 2021; published 4 October 2021)

Eliminating the effect of residual infrared absorption in titanium sapphire remains a crucial task to fulfill, despite that this kind of laser crystal has been developed for decades. The Ti^{3+}-Ti^{4+} (Ti^{0}_{Al}-Ti^{1+}_{Al}) pair model is the most widely accepted explanation to this residual absorption, but theoretical analyses based on first-principles calculation have not yet depicted a clear picture for the variation of the Ti^{0}_{Al}-Ti^{1+}_{Al} pair and a variety of other potentially important defects in titanium sapphire when fabricating conditions change. Here, we extend the work in [W. Jing, M. Liu, J. Wen, L. Ning, M. Yin, and C.-K. Duan, Phys. Rev. B **104**, 165103 (2021)] about binding tendencies of Ti_{Al}-Ti_{Al} pairs and optical transition properties to providing a comprehensive understanding of the formation and processing condition dependence of various potentially significant defects and complexes besides the $(Ti_{Al}\text{-}Ti_{Al})^{0,1+}$ pairs. Apart from the complexes composed of V^{3-}_{Al} and $Ti^{0,1+}_{Al}$ defects, two new significant negatively charged defects, $(V_{Al}\text{-}Al_i\text{-}V_{Al})^{3-}$ and $(V_{Al}\text{-}Ti_i\text{-}V_{Al})^{2-}$ are revealed. These two complexes are correspondingly an interstitial Al^{3+} and Ti^{4+} surrounded by two neighboring aluminium vacancies V^{3-}_{Al}. We show that V^{3-}_{Al} plays the key role to stabilize Ti^{0}_{Al}-Ti^{1+}_{Al} and form various stable complexes with Ti^{1+}_{Al} and Ti^{0}_{Al}-Ti^{1+}_{Al} in weak and moderate reductive atmospheres. Thus, besides annealing at strong reductive atmosphere at elevated temperatures, Al ion injection or annealing in Al vapor is a potential method to eliminate the harmful residual infrared absorption, which is pinpointed at the reduction of the concentration of V^{3-}_{Al} and its variant $(V_{Al}\text{-}Al_i\text{-}V_{Al})^{3-}$. While in extremely strong reductive atmosphere, isolated Ti substitution dominates over those complexes containing V^{3-}_{Al}, but there still remains a tiny amount of Ti^{0}_{Al}-Ti^{1+}_{Al} and Ti^{1+}_{Al}, which are charge compensators to balance the charge of trace amount Ti^{1-}_{Al} further reduced from Ti^{0}_{Al}. And this effect can be further eliminated by lower temperature reductive-atmosphere annealing. In addition, we obtain a simple numerical expression to predict the achievable figure of merit when the concentration of Ti^{1+}_{Al} is given. Formation energies for simple defects and binding energies for complexes obtained in this work may serve as the basis for simulations and design various quenching and annealing processes to further reduce harmful defect species in titanium sapphire.

DOI: 10.1103/PhysRevB.104.165104

I. INTRODUCTION

Titanium sapphire ($Ti:Al_2O_3$) is one of the most important laser crystals that scientific and medical researches for this material have been carried out over decades [1–6]. The emission band extending from 600 to about 1100 nm, which is originated from vibronic transitions between $3d$ Stark levels of Ti^{3+} ions due to strong ligand field interaction [7,8], provides a wide tuning range and high gain cross section [9]. To improve the performance of the $Ti:Al_2O_3$ laser crystal, there are extensive experimental and theoretical studies for decades on the defects in $Ti:Al_2O_3$ and their spectroscopic properties [10–17]. And one of the well-known unsolved problem is how to eliminate the so-called residual infrared absorption [18] whose broad absorption band is centered near 800 nm, exactly the lasing wavelength range, and extremely restricts the laser performance [5]. Recently, Moulton *et al.* [5,10] have carried thorough spectroscopic measurements in the UV-near-IR (190–2000 nm) ranges over a large variety of different concentration samples from various sources grown by several techniques and post-processed under different conditions [10], and they study the impact of various absorption on optical pumping of the Ti:sapphire laser [5]. Many different absorption features in the spectrum range have been revealed and characterized. It is concluded that further theoretical modeling the energy levels of different complexes in Ti:sapphire should be done to examine Ti^{3+}-Ti^{4+} (i.e., Ti^{0}_{Al}-Ti^{1+}_{Al}) pair model and to explain the effects of Ti^{1+}_{Al}, V^{3-}_{Al} and other defects [10].

*ckduan@ustc.edu.cn

The first-principles calculation based on density functional theory (DFT) [19–22] provides a powerful tool to understand the residual infrared absorption, and the DFT method has been applied to study the variation of concentrations about doped Ti ions and their complexes with intrinsic defect of Al_2O_3 under various growth conditions and annealing processes [13,17,23]. However, these works may suffer the negligence of delocalization error for $3d$ electrons of Ti atoms, which overestimate the binding energies of Ti_{Al}^{0}-Ti_{Al}^{0} and Ti_{Al}^{0}-Ti_{Al}^{1+}, and predict unreasonable high aggregation concentrations of these two defects.

In this paper, we aim to provide a comprehensive study about the potentially important defects and complexes in the Ti:Al_2O_3 crystal based on the well-determined DFT approach in Ref. [24]. Experiments show that Ti:Al_2O_3 is a good laser material and the clustering tendency is not serious in this material under appropriate fabricating conditions. Thus, to determine all potentially significant complexes, we firstly consider all the simple defects in Ti:Al_2O_3 like intrinsic defects of α-Al_2O_3, Ti substitution (denoted as Ti_{Al}) and Ti interstitial (denoted as Ti_i). Then we suppose that significant complexes are due to clustering of those significant simple defects, while the combination of the more energetic simple defects are ignored unless there is a large Coulomb attraction to counteract their disadvantages on energy.

According to our self-consistent concentration calculation to those simple defects, we find that Al vacancy V_{Al}^{3-} and Ti substitution $Ti_{Al}^{0,1+}$ play the major roles in Ti:Al_2O_3 under all chemical synthesis conditions under consideration. Therefore, when complexes are introduced to the concentration calculation, the combination of a V_{Al}^{3-} with one or several surrounding $Ti_{Al}^{0,1+}$ defects should be the most significant complex structures besides $(Ti_{Al}\text{-}Ti_{Al})^{0,1+}$ pairs, and Coulomb attractions between V_{Al}^{3-} and Ti_{Al}^{1+} benefit this kind of clustering too.

Actually, this kind of V_{Al}^{3-} and $Ti_{Al}^{0,1+}$ related cluster has also been considered in previous DFT calculations [13,17,23]. In addition, experiments provide some evidences for the existence of clustering V_{Al}^{3-} with several $Ti_{Al}^{0,1+}$. Yamaga *et al.* suggested that there is a charge compensating V_{Al}^{3-} at a neighboring site of Ti_{Al}^{0}-Ti_{Al}^{1+} cluster [25]. And a more recent experiment indicates that not only the cluster V_{Al}^{3-} with three Ti_{Al}^{1+} should be considered, V_{Al}^{3-} with one or two Ti_{Al}^{1+} are also important in Ti:Al_2O_3 crystal by comparing Al self-diffusion in high-purity α-Al_2O_3 with Ti:Al_2O_3 [26].

Although there are some indications for the existence of Ti_i^{3+} in Ti:Al_2O_3 crystal [27], both our DFT and previous calculations [11] show that the concentration of isolated $Ti_i^{3+,4+}$ can be neglected because of its large formation energy. However, this result does not rule out the existence of Ti_i complex in Ti:Al_2O_3 crystal. Actually, we show a new cluster composed of a Ti_i and two nearest-neighbor Al vacancies (V_{Al}^{3-}) can be stable and exist in crystal with a sizable concentration. And this complex prompts us to find a new type of V_{Al}^{3-}, which leads to the Schottky disorder with a formation energy more compatible with experimental measurements. All these will be discussed in detail in Sec. III A.

Once all the significant defects and complexes are determined, we illustrate our consideration to simulate fabricating conditions and important annealing processes. Experiments have already known that more favorable Ti:Al_2O_3 crystal should be annealed at reduction atmosphere and elevated temperature near the melt point of Al_2O_3. However, extremely reductive atmosphere is always hard to obtain under high temperature, which restricts further improvement of Ti:Al_2O_3 crystal. Thus lower annealing temperature with stronger reducing atmosphere might be another possible choice. Nevertheless, thermodynamic equilibrium distribution for concentrations of defects and complexes might not be reached if the temperature is too low to activate the motion of compositions to form or decompose a complex. Thus we set the annealing temperature at 1873 K, i.e., approximately 80% of the melting point and assume that equilibrium distribution of various defects in Ti:Al_2O_3 can be achieved at such temperature due to Al atom diffusion study in experiment [26]. More detail about how to calculate the thermodynamic equilibrium distribution for concentrations of defects and complexes can be found in Sec. II B.

Based on our calculation, we eventually provide in Sec. III E an insight for previously experimental guidance in Ref. [28] about improving the figure of merit (FOM) in Ti:Al_2O_3 lasers, and we further provide an estimation of achievable FOM when the concentration of Ti_{Al}^{1+} is known in experiment. Moreover, we will also try to derive the approximate square law between the concentration of Ti_{Al}^{0}-Ti_{Al}^{1+} pair and Ti_{Al}^{0} as reported in Ref. [17]. Finally, we conclude our study by putting forward proposals on substantially eliminating the harmful residual infrared absorption.

II. METHODOLOGY

A. Computational procedure

The first-principles calculation based on DFT are performed by using the VASP code [29–32], where the plane-wave basis set is adopted to expand the eigen wave function, and project augment wave (PAW) pseudopotentials are used to describe the interactions of atoms [33,34]. For the exchange-correlation term in DFT, the PBEsol version of GGA functional whose parameters are specifically optimized for crystal [35,36] and the Hubbard U correction, namely the DFT+U method, has been adopted to consider the localization effect of the d electron in transition element by applying the U value-related correction in the exchange-correlation functional [37,38]. We choose $U = 4$ eV for the $3d$ electron of Ti ions in Ti:Al_2O_3 by requiring the density functionals to fulfill the generalized Koopmans condition [39,40], and the detail can be found in Ref. [24].

During the structure relaxation of α-Al_2O_3 primitive cell (space group R-$3c$), the original structure comes from Inorganic Crystal Structure Database (ICSD) with code 26790, and the crystal lattice and atomic positions are fully relaxed by using a $9 \times 9 \times 9$ k-point sampling of the Brillouin zone. Furthermore, spin-polarized calculations were performed for rutile TiO_2, α-Ti metal, and isolated O_2 molecule and single oxygen atom in 10^3 Å^3 cubic cells to provide references for or constraints on chemical potentials. The supercell method is employed to calculate the total energy of potential defects in Ti:Al_2O_3 crystal. To obtain defect and complex formation energy in isolated limit, extrapolation method is adopted and

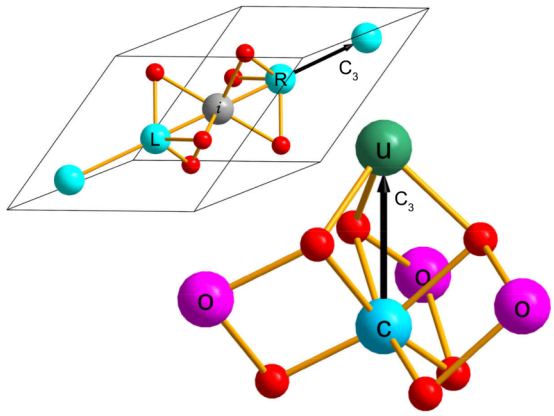

FIG. 1. Top left: the modified primitive cell of Al_2O_3 containing a Ti_i (or Al_i) in the center. Bottom right: the basic unit to visualize multiple complex defects. The primitive cell without Ti_i (or Al_i) contains four Al atoms in blue color along the C_3 axis and six oxygen atoms in red forming a distorted octahedron. The basic unit includes the center Al site (blue and denoted as c site) and four surrounding neighbors of Al site including one nearest neighbor (green and denoted as u site) and three next neighbors (purple and denoted as o site). The arrow from the center Al to its nearest neighbor Al is the C_3 axis. It is noted that there is only one inequivalent single Al site and c, u and o are just used to distinguish inequivalent positions in a complex.

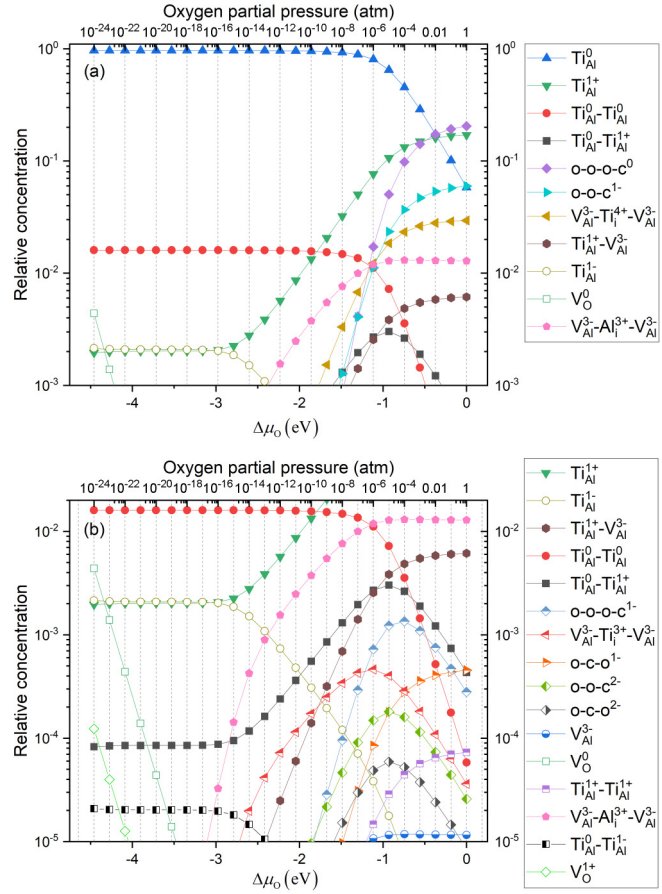

FIG. 2. The relative concentration at equilibrium of the dominant (a) and other less dominant but important (b) defects and complexes in Ti:Al_2O_3 crystal. The total Ti concentration is fixed at 0.50 at.% (2.34×10^{20} cm^{-3} or 0.47 wt.%) and is used to normalize the concentrations of others. The annealing temperature is set at 1873 K. It is noted that Eq. (11) suggests a rescaling of the pressure by a factor 2.2×10^{-4}. For compact and accurate display, the equilibrium concentrations of similar complexes are merged by ignoring the difference between u and o site in configuration, i.e., by treating u and o sites as the same. In addition, relationships between formation energies of these defects and complexes and the Fermi level in a given oxygen partial pressure can be referred in Sec. S4 [41].

a series of supercells containing 120, 180, 380, and 960 atoms are constructed by expanding our relaxed primitive cell and their sizes and shapes are fixed during the structure relaxation. Furthermore, single Γ point integration is adopted in the Brillouin zone because as the dominant supercells are big enough. The plane-wave cutoff energy is set at 520 eV in the structure optimization of primitive cell, while a smaller cutoff energy of 400 eV is used in all defects-related calculations as a compromise between the calculation accuracy and computational costs. In all structure relaxations, the total energy variation for each system is converged to 10^{-3} meV/atom and the absolute residual force for each atom is less than 5 meV/Å.

To test the influence about the Γ point integration on the formation energies of the main defects in Fig. 2(a), the k-point mesh grids are set as $2 \times 3 \times 4$, $3 \times 3 \times 3$, $3 \times 4 \times 4$, $3 \times 4 \times 5$, and $5 \times 5 \times 5$ for 120-atom supercell, while for 180- and 380-atom supercells, calculations are obtained by integrating over $2 \times 3 \times 4$, $3 \times 3 \times 3$, $3 \times 4 \times 5$ grids of k points. Our calculation shows that, for a given defect, the difference between doped supercell and corresponding pristine bulk, namely, the relative formation energy, depends only weakly on k-point mesh grids and the shape of supercell. Specifically, the Γ point integration will introduce less than 0.05 eV uncertain for formation energies of dominant defects in extrapolation method. The details can be found in Ref. [41], Sec. S1.

We have also checked the local structures of each defect in supercells of different size, and find that they are all fully relaxed and the variation between 120-atom and 960-atom supercells similar to the results in Ref. [24] whose influence to extrapolated formation energy can be neglected. We use one of the largest complex both in size and charge to illustrate it (see Sec. S2 of Ref. [41] for a detailed discussion on this).

B. The self-consistent concentration calculation of defects and complexes

Based on Refs. [42–44], the formation energy of isolated defect or complex X in charge state q can be written as follows:

$$E_f(X^q, E_F) = [E_{\text{tot}}(X^q) + E_{\text{corr}}(X^q)] - E(\text{bulk}) - \sum_i \Delta n_i \mu_i + qE_F. \quad (1)$$

In this expression, $E_{\text{tot}}(X^q)$ is the total energy of the supercell containing a X^q defect or complex and $E_{\text{corr}}(X^q)$ is the correction required to extrapolate $E_{\text{tot}}(X^q)$ to the dilute limit, and

E(bulk) is the total energy of corresponding pristine supercell. Δn_i means the number change of i-type atoms between doped structure and the host, i.e., if $\Delta n_i > 0$ ($\Delta n_i < 0$), i-type atoms are added to (removed from) the supercell when the defect or complex structure is created, and μ_i corresponds to the chemical potential of this species which depends on the fabrication condition. The term $E_F \equiv \varepsilon_{\mathrm{VBM}} + \Delta\varepsilon_F$ represents the Fermi level, where $\varepsilon_{\mathrm{VBM}}$ is the valence-band maximum (VBM) of the host. In the supercell method with periodic boundary condition, the formation energy of X^q depends on the size of supercell and the correction E_{corr} should be considered because of the well-known electrostatic image-charge interaction and the neglect of the average potential difference between doped and pristine supercells [44].

Regarding to the charge and supercell-size related correction in Eq. (1), the extrapolation method is adopted to directly obtain the formation energy of X^q in isolated limit, $E_f(L \to \infty)$. According to the study of Castleton *et al.* [45], the fitting curve for the formation energy over near cubic supercells satisfies

$$E_f(L) = E_f(L \to \infty) + \frac{a_1}{L} + \frac{a_3}{L^3}, \tag{2}$$

where L is the length scale of the supercell so defined that L^3 equals the volume of the supercell, and a_1 and a_3 are fitting parameters. In this work, the 120, 180, 380, and 960 atoms supercells are used, and the detail about fitting method and building the supercell close to the cubic shape can be referred from Ref. [24].

For a given defect, the higher Fermi level favors the defect with the lower charge in formation energy and concentration. The thermodynamic charge transition level $\varepsilon(X, q_2/q_1)$ is defined as the Fermi level that equalizes the formation energy of X^{q_1} and X^{q_2} [43], i.e.,

$$\varepsilon(X, q_2/q_1) = -\frac{E_f(X^{q_2}, 0) - E_f(X^{q_1}, 0)}{q_2 - q_1}. \tag{3}$$

It is noted that the right-hand side actually only depends on the (corrected) total energy and the charge differences of the defects between the two different charge states. $\varepsilon(X, q_2/q_1)$ is often given relative to $\varepsilon_{\mathrm{VBM}}$ for convenience.

In thermodynamic equilibrium, the relation between formation energy E_f and concentration c of defect or complex is [42]

$$c = \omega N \exp(-E_f/kT). \tag{4}$$

Here, N is the number of sites in the lattice (per unit volume) available for the defect or complex, k is Boltzmann's constant and T is the temperature. Finally, ω is degeneracy factor, i.e., the intrinsic degree of freedom for defect or complex structure.

Phase diagram is a commonly used method to constrain the chemical potentials, and different extremes in the phase diagram are used to analysis the range of concentrations of defects and complexes. The chemical potentials of Ti, Al, and O will be constrained by various phase equilibrium conditions related to the fabricating processes [13,17]. However, in this work, we are more interested in the variation of the concentrations of various defects and complexes under continuous variation of reductive atmosphere and temperature in annealing.

From Eqs. (1) and (4), for a given temperature, the concentration of defect or complex X^q in Ti:Al_2O_3 is the function of chemical potential μ_{Ti}, μ_{Al}, μ_{O}, and Fermi level E_F. Due to the low doping concentration of Ti in Ti:Al_2O_3 that is usually concerned, we suppose that the doping only weakly influences the chemical potentials of Al and O, hence $2\mu_{\mathrm{Al}} + 3\mu_{\mathrm{O}} = g^{\mathrm{bulk}}_{\mathrm{Al_2O_3}}$ is still satisfied, where the $g^{\mathrm{bulk}}_{\mathrm{Al_2O_3}}$ is the Gibbs free energy of bulk Al_2O_3 and is approximately taken as the calculated total energy $E^{\mathrm{bulk}}_{\mathrm{Al_2O_3}}$ [43]. When the reductive atmosphere is given, i.e., μ_{O} is known, the value of μ_{Al} can be determined correspondingly. Meanwhile, the concentration of a defect or complex is just the function of μ_{Ti} and E_F, but these two parameters are not independent. By considering all possible defects and complexes in Ti:Al_2O_3 crystal, concentrations of these defects and complexes, $\{c(X^q)\}$, should satisfy the condition of charge neutrality [43]

$$\sum_{X^q} c(X^q)\, q + n_h - n_e = 0, \tag{5}$$

where n_h and n_e are concentrations of free holes in VB and electrons in CB. And the difference between n_e and n_h can be further approximated as

$$n_e - n_h = 2\left(\frac{m_e k_{\mathrm{B}} T}{2\pi\hbar^2}\right)^{3/2} \exp\left[(E_F - \varepsilon_{\mathrm{CBM}})/k_{\mathrm{B}}T\right] - 2\left(\frac{m_h k_{\mathrm{B}} T}{2\pi\hbar^2}\right)^{3/2} \exp\left[(\varepsilon_{\mathrm{VBM}} - E_F)/k_{\mathrm{B}}T\right], \tag{6}$$

m_e and m_h are effective mass of electron and hole respectively, $\varepsilon_{\mathrm{VBM}}$ and $\varepsilon_{\mathrm{CBM}}$ are VBM and CBM position of Al_2O_3 bulk which have been obtained from HDFT calculations in Ref. [24].

The total doped Ti concentration c_{Ti} brings about the following constraint:

$$\sum_{X^q} c(X^q)\, k(X^q) = c_{\mathrm{Ti}}, \tag{7}$$

where $k(X^q)$ is the number of Ti ions in X^q. Hence, the concentrations of all considered defects and complexes can be determined self-consistently when fabricating conditions, i.e., the processing temperature, chemical potential μ_{O} and the total doping concentration of Ti are specified.

III. RESULTS AND DISCUSSIONS

A. The introduction about geometric structures of complexes

The bottom right of Fig. 1 shows the basic unit to construct complexes about binary $\mathrm{Ti_{Al}}$-$\mathrm{Ti_{Al}}$, $\mathrm{Ti_{Al}}$-V_{Al}, ternary $\mathrm{Ti_{Al}}$-$\mathrm{Ti_{Al}}$-V_{Al} and quaternary $\mathrm{Ti_{Al}}$-$\mathrm{Ti_{Al}}$-$\mathrm{Ti_{Al}}$-V_{Al}. This basic unit includes a center Al site (blue and denoted as c site) with its surrounding four Al sites including one nearest neighbor (green and denoted as u site) and three next neighbors (purple and denoted as o site). The arrow from the center Al to its nearest neighbor Al is the C_3 axis. It is noted that all Al site are equivalent in α-Al_2O_3 crystal and c, u and o are just used to distinguish inequivalent relative positions in a given basic unit to form the complex. For binary $\mathrm{Ti_{Al}}$-$\mathrm{Ti_{Al}}$, $\mathrm{Ti_{Al}}$-V_{Al} complexes, we only consider center Al site with its nearest neighbor or one of three next nearest neighbor Al sites to form these binary complexes, and we can use c-u and c-o configurations to denote these two different geometry structures.

As for the interstitial titanium ion (Ti_i), only charge states +3 and +4 are considered because these two commonly states for Ti ions in Ti:Al_2O_3 crystal. It is well-known that there are many potential interstitial sites in a given supercell and enumerating all these possible sites in a supercell is not an easy task. So we follow the hypothesis in Ref. [46] that all possible sites should be located at or near the corner, edge and face center of the Voronoi polyhedra constructed in the supercell and the algorithm implementation can be referred from Ref. [46] or the codes [47]. Based on this method, we determine the most probable interstitial site by structure optimization and choosing the one having the minimum total energy from all candidate sites we generated. And the most stable interstitial site for $Ti_i^{3,4+}$ has been shown in the upper left of Fig. 1, which is along the C_3 axis of the crystal and exactly locates at the center of the primitive cell.

Our calculation finds that although single $Ti_i^{3,4+}$ never dominates in any of the fabricating conditions we are concerned (many orders of magnitude smaller than $Ti_{Al}^{0,1+}$ even for the rich titanium and poor aluminium extreme), the combination between charged $Ti_i^{3,4+}$ and V_{Al}^{3-} can greatly reduce the complex's formation energy as a result of strong Coulomb attraction, leading to the stable complex $(V_{Al}\text{-}Ti_i\text{-}V_{Al})^{3,2-}$, i.e., $Ti_i^{3,4+}$ associated with two vacancies at its two nearest neighbor Al sites.

Actually, we have considered the combination of $Ti_i^{3,4+}$ with only one nearest neighbor V_{Al}^{3-} as $(Ti_i\text{-}V_{Al})^{0,1+}$, but we find that the configurations of $(Ti_i\text{-}V_{Al})^{0,1+}$ is not very stable in that $Ti_i^{3,4+}$ can easily cross a small barrier [≈0.12 eV for $(Ti_i\text{-}V_{Al})^0$, 0.14 eV for $(Ti_i\text{-}V_{Al})^{1+}$] and move to V_{Al}^{3-} site to form the more favorable simple defect $Ti_{Al}^{0,1+}$. While for the complex $(V_{Al}\text{-}Ti_i\text{-}V_{Al})^{3,2-}$, its formation energy is smaller than $(V_{Al}\text{-}Ti_{Al})^{3,2-}$ by ≈1.3 eV/1.5 eV and there is a barrier $\lesssim$2.8 eV/3.3 eV between $(V_{Al}\text{-}Ti_i\text{-}V_{Al})^{3,2-}$ and $(V_{Al}\text{-}Ti_{Al})^{3,2-}$ (see Fig. S3 in Sec. S3 of Ref. [41] for the potential surface curves).

Similarly, replacing the Ti_i^{3+} in $(V_{Al}\text{-}Ti_i\text{-}V_{Al})^{3-}$ with Al_i^{3+} leads to a new complex $(V_{Al}\text{-}Al_i\text{-}V_{Al})^{3-}$ which is lower by 1.24 eV in formation energy than the simple V_{Al}^{3-}. Actually, $(V_{Al}\text{-}Al_i\text{-}V_{Al})^{3-}$ can be viewed as a variant of the single V_{Al}^{3-} from Fig. 1: when one of the aluminum ion near the center is removed and the other is displaced along the C_3 axis to the center, $(V_{Al}\text{-}Al_i\text{-}V_{Al})^{3-}$ is formed. Actually, the migration of a simple V_{Al}^{3-} at site L (upper left of Fig. 1 but removing interstital ion i) to site R can be viewed as the Al ion at site R in the defect V_{Al_L} configuration moves to site i to form the $V_{Al_L}\text{-}Al_i\text{-}V_{Al_R}$ configuration, and then the Ai_i recombines with V_{Al_L}, with only V_{Al_R} left (see Fig. S3 in Sec. S3 for the two energy barriers [41]). In addition, just like $(Ti_i\text{-}V_{Al})^0$ complex, we also find that $(Al_i\text{-}V_{Al})^0$ is not stable. The barrier for Al_i^{3+} moving towards V_{Al}^{3-} is about 0.22 eV and the detail for $(Al_i\text{-}V_{Al})^0$ potential surface curves can be referred in Sec. S3 [41].

B. The configurations, charge corrections, and formation or binding energies of defects and complexes

Table I lists the configurations of potentially significant defects and N_{config} as the number of available sites per primitive cell. For each V_{Al} or Ti_{Al}, there are four equivalent Al sites per primitive cell for doping, so $N_{config} = 4$, and these simple defects only have one way to occupy a given Al site, so the degeneracy factor $\omega = 1$. Nevertheless, as for complexes, it might be hard to count the number of N_{config} and ω in an intuitive way. Thus we provide a more general method to avoid these tame tasks by using the group theory [48].

The space group G of α-Al_2O_3 is R-3c (No. 167). There are 12 times of the lattice translational operations n for this space group, which we shall denote as $[G] = 12n$. As for binary Ti_{Al}-Ti_{Al} and Ti_{Al}-V_{Al}, we firstly have to figure out the number of sites allowed to occupy, i.e., how many adjacent Al-Al pairs in the crystal. If these two Ti ions are nearest neighbors (denoted as u-c in Fig. 1), the point group g for operations to keep this configuration unchanged is D_3, which contains six operations, while the rest operations in G will move this u-c configuration to other positions, i.e., the equivalent but not the original sites for binary defects doping. Thus the total number of u-c configurations in the crystal is $[G]/[g] = 12n/6 = 2n$. Then the number of u-c configurations per primitive cell equals $2n/n = 2$. As for the next nearest neighbor configuration of Ti pair (denoted as o-c), the point group is $C_i = S_2$ of 2 operations, so $N_{config} = 6$ for o-c. After the number of sites which are allowed to accommodate the complex has been figured out, we further consider how a complex may occupy one given site. As for Ti_{Al}-Ti_{Al}, there is only one way to form the u-c or o-c configuration due to the identity of Ti ions, so $\omega = 1$. While in the Ti_{Al}-V_{Al} complex, $\omega = 2$.

For multiple complex defects Ti_{Al}-Ti_{Al}-V_{Al} and Ti_{Al}-Ti_{Al}-Ti_{Al}-V_{Al}, they occupy the basic unit shown in Fig. 1 and the point group of this unit is C_3, so $N_{config} = 4$, but ω varies. Table I lists every situation how a complex occupy the unit structure. Here we take the u-o-c-o configuration in Ti_{Al}-Ti_{Al}-Ti_{Al}-V_{Al} as an example to illustrate the calculation of ω, three Ti ions occupy sequentially u, o, and c sites, while V_{Al} occupies the last o site in u-o-c-o configuration, i.e., the u and c sites are uniquely occupied by two Ti ions while three o sites are occupied by Al, Ti, and V_{Al} with $3! = 6$ permutations, leading to $\omega = 6$.

The valence of Ti in a cluster needs to be taken into account, an extra valence-related factor in ω is required to describe the rearrangement of Ti_{Al}^0 and Ti_{Al}^{1+} in equivalent sites of the cluster when the configuration is given. For example, for each Ti_{Al}^0-Ti_{Al}^{1+}, this factor is 2, and for each Ti_{Al}^0-Ti_{Al}^{1+}-Ti_{Al}^{1+}-V_{Al}^{3-} or Ti_{Al}^0-Ti_{Al}^0-Ti_{Al}^{1+}-V_{Al}^{3-} in o-o-o-c configuration, the extra valence-related factor is 3.

Moreover, for open-shell valence state of a simple defect or cluster, the usually-ignored degeneracy of the electronic state contributes an additional factor to ω. For all the defects considered in this work, the spin-orbit coupling is small, so that the degeneracy of the ground energy level is the product of its spin multiplicity $2S + 1$ and the degeneracy of its space wave function. The latter, if not one, is usually lifted due to geometric relaxation (e.g., Jahn-Teller effect). Our calculations show that the exchange interaction between two simple defects such as between two Ti^{3+} or Ti^{2+} and Ti^{3+} are less than 0.05 eV and so parallel and antiparallel cases are considered as degenerate. Under this approximation, the spin-degeneracy factor can be simplified as a product of several factors as follows: for each Ti^{4+}, Ti^{3+}, Ti^{2+} in a defect, includes a spin-multiplicity factor correspondingly $2S + 1 = 1,\ 2,\ 3$;

TABLE I. The configuration, the image-charge correction in $E_{\rm corr}$ for the 120-atom supercell, and $E_{\rm b}$ of defect X^q in the dilute limit.[a]

Defect	Occupied sites	Degeneracy factor ω[b]	$N_{\rm config}$	$E_{\rm corr}(X^q)$ (eV)			$E_{\rm b}(X^q)$ (eV)			
				$\lvert q\rvert=1$	$\lvert q\rvert=2$	$\lvert q\rvert=3$	$q=0$	$\lvert q\rvert=1$	$\lvert q\rvert=2$	$\lvert q\rvert=3$
$V_{\rm Al}$	c	1	4	0.44	1.19	2.43	3.74	4.37	5.59	7.42
$V_{\rm Al}$-Al$_i$-$V_{\rm Al}$	/	1	2		0.83	1.76			4.59	6.25
$V_{\rm O}$	/	1	6	0.13	0.40		7.59	4.86	2.41	
$\rm Ti_{Al}$	c	1	4	0.13(+), 0.15(−)			2.45	−0.08(+), 6.92(−)		
$\rm Ti_{Al}$-$\rm Ti_{Al}$	u-c	1	2	0.02	0.22		−0.12	−0.05	0.35	
	o-c	1	6	0.03	0.22		−0.07	−0.07	0.34	
$\rm Ti_{Al}$-$V_{\rm Al}$	u-c	2	2	0.58	1.44	2.65	−1.20	−1.52	−1.99	−0.17
	o-c	2	6	0.55	1.43	2.55	−1.04	−1.42	−1.90	−0.32
$V_{\rm Al}$-Ti$_i$-$V_{\rm Al}$[c]	/	1	2		0.66	1.69			−2.52	−1.61
$\rm Ti_{Al}$-$\rm Ti_{Al}$-$V_{\rm Al}$	o-o-c	3	4	0.66	1.57	2.87	−2.56	−3.45	−2.11	−0.50
	u-o-c	3	4	0.74	1.63	2.90	−2.53	−3.23	−2.12	−0.29
	u-o-o	6	4	0.80	1.59	2.81	−1.33	−1.87	−1.37	−0.08
	o-o-o	3	4	0.78	1.56	2.39	−1.13	−1.66	−1.16	−0.30
	u-c-o	3	4	0.82	1.65	2.86	−1.92	−2.51	−1.86	−0.37
	o-c-o	6	4	0.75	1.56	2.79	−1.70	−2.31	−1.82	−0.21
	o-o-u	3	4	0.81	1.66	2.85	−1.66	−2.17	−1.19	0.12
	o-c-u	3	4	0.78	1.61	2.85	−2.03	−2.58	−1.81	−0.10
	o-o-o-c	1	4	0.56	1.81	3.03	−4.40	−3.69	−2.28	−0.57
	u-o-o-c	3	4	0.75	1.79	3.06	−4.82	−3.72	−2.38	−0.83
	u-o-o-o	3	4	0.66	1.49	2.69	−2.32	−2.08	−1.64	−0.40
$\rm Ti_{Al}$-$\rm Ti_{Al}$-$\rm Ti_{Al}$-$V_{\rm Al}$	u-o-c-o	6	4	0.62	1.65	2.72	−2.84	−2.70	−1.88	−0.54
	o-o-c-o	3	4	0.56	1.51	2.94	−2.76	−2.66	−2.11	−0.43
	o-o-o-u	1	4	0.59	1.62	2.86	−2.97	−2.25	−1.23	0.01
	o-o-c-u	3	4	0.58	1.44	2.73	−3.07	−2.66	−1.64	−0.19

[a]It is noted that (1) these $V_{\rm Al}$-containing defects with $|q|\neq 0$ are negatively charged; (2) for simple defects $V_{\rm Al}$ and its variant $V_{\rm Al}$-Al$_i$-$V_{\rm Al}$, $V_{\rm O}$ and $\rm Ti_{Al}$, $E_{\rm b}$ here actually refers to the extrapolated defect formation energy $E_f(L\to\infty)$ in Eq. (2) and the reference chemical potentials $\mu_{\rm O}=E_{\rm O_2}/2$, $2\mu_{\rm Al}+3\mu_{\rm O}=E_{\rm Al_2O_3}$, $\mu_{\rm Ti}+2\mu_{\rm O}=E_{\rm TiO_2}$ and $E_F=\varepsilon_{\rm VBM}$ of GGA are adopted in Eq. (1); (3) for complexes, $E_{\rm b}$ values are binding energies derived from $E_f(L\to\infty)$ with Eq. (8), and are independent of chemical potentials and the Fermi energy; (4) some clusters or valence states in Fig. 3 (such as clusters containing $\rm Ti_{Al}^{1-}$) are omitted here, as their influence are not important as Fig. 2 illustrated.
[b]The extra valence-related factor and electronic state degeneracy are not included here, see main text for explanation.
[c]The binding energy of this defect is calculated relative to $V_{\rm Al}^{3-}$ and $\rm Ti_{Al}$.

for $V_{\rm Al}^q$ or its variant $(V_{\rm Al}\text{-Al}_i\text{-}V_{\rm Al})^q$ ($q=-3,\ -2,\ -1,\ 0$), includes $2S+1=1,\ 2,\ 3,\ 4$ correspondingly, and for each $V_{\rm O}^q$ ($q=2,\ 1,\ 0$), includes $2S+1=1,\ 2,\ 1$.

For a complex defect, we define the binding energy as the energy required to form the complex from simple defects, i.e.,

$$E_{\rm b}(AB^{q_1+q_2})=E_f(AB^{q_1+q_2})-[E_f(A^{q_1})+E_f(B^{q_2})], \quad (8)$$

where $E_f(AB^{q_1+q_2})$, $E_f(A^{q_1})$, and $E_f(B^{q_2})$ are the formation energies for complex $AB^{q_1+q_2}$, simple defects A^{q_1} and B^{q_2} in the dilute limit ($L\to\infty$), respectively. It is noted that the binding energies are independent of chemical potentials and the Fermi energy, as these quantities are canceled out in Eq. (8).

In connection to the formation energy, it is straightforward to obtain from Eq. (4) that the factor $\exp(-E_b/kT)$ reflects the tendency of aggregation of A^{q_1} and B^{q_2} to $AB^{q_1+q_2}$ in that the relative concentration $c_a/(\omega_a N_a)$ [$a=AB^{q_1+q_2}$] is enhanced over the product of $c_1/(\omega_1 N_1)$ [1 being A^{q_1}] and $c_2/(\omega_2 N_2)$ [2 being B^{q_2}] by the factor $\exp(-E_b/kT)$. Hence, positive $E_{\rm b}$ means that energy is required to form this complex and it prefers to decompose to isolated defects, while a negative value means the formation of a complex is favorable and its aggregation is enhanced.

Table I lists the image-charge correction of each charged defect at different configurations in the 120-atom supercell, and correspondingly the corrected formation energy for simple defects obtained via Eq. (1) together with Eq. (2) or the binding energies $E_{\rm b}$ obtained by Eq. (8) for complexes. It is noted that, in calculating the formation energies, the reference values for chemical potential $\mu_{\rm O}=E_{\rm O_2}/2$, $2\mu_{\rm Al}+3\mu_{\rm O}=E_{\rm Al_2O_3}$, $\mu_{\rm Ti}+2\mu_{\rm O}=E_{\rm TiO_2}$, and $E_F=\varepsilon_{\rm VBM}$ are adopted.

The formation energies for simple defects and binding energies for complexes in Table I allow to calculate the formation energies of all defects for any given chemical potentials of elements and Fermi energy from Eq. (1) together with Eq. (8).

It is worthy noting that even for the same complex species but distinctive configurations, as shown in Table I, the image-charge corrections can be quite different, not to mention the remarkable distinguish in the corrections for two different complex merely with the same charge. For example, the charge correction for the complex $(V_{\rm Al}\text{-Ti}_i\text{-}V_{\rm Al})^{3-}$, which has a more balanced charge distribution than $(\rm Ti_{Al}$-$V_{\rm Al})^{3-}$, is 1.69 eV, but takes a much larger value of 2.65 eV for

$(Ti_{Al}\text{-}V_{Al})^{3-}$ at *o-c* configuration. Hence, it is important that the extrapolating method has been used instead of a simple point-charge correction with a potential alignment correction. Moreover, for a given complex species, if we suppose that the deviation of image-charge corrections among different configurations is an indication of the level of extrapolation error when they are considered as the same defect, the uncertainty of image-charge corrections is ≈0.1 eV for $|q| = 1$ or 2 and ≈0.2 eV for $|q| = 3$.

C. The concentration of defects in titanium-doped alumina in different chemical environment

As discussed in Sec. II B, the variation of concentrations of potentially significant defects with the reductive condition specified by the chemical potential of oxygen can be determined for any given temperature and the total concentration of Ti ions. Usually, the total concentration of Ti ion in Ti:Al_2O_3 is on the order of 10^2–10^3 ppm of Al site, despite that a crystal at the high concentration of 0.41 at.% was developed in Ref. [49]. To show the influence of aggregation of dopants and intrinsic defects, we consider a fairly large concentration of Ti ion at 0.5 at.%, i.e., 2.34×10^{20} cm^{-3} or 0.47 wt.%, and we set the annealing temperature at 1873 K. The results are plotted in Fig. 2.

We note that most of the significant complexes by concentration in Ti:Al_2O_3 have $|q| = 1$, as shown in Fig. 2, and our test shows that an error of ±0.1 eV in the formation energy of $o\text{-}o\text{-}c^{1-}$ will affect the concentration of $Ti_{Al}^{0}\text{-}Ti_{Al}^{1+}$ by about ∓10 %, while ±0.1 eV in the formation energy of $Ti_{Al}^{0}\text{-}Ti_{Al}^{1+}$ will lead to down- or up-scaling its concentration by a factor $\lesssim 2$. For other complexes, image-charge corrections may suffer similar fitting errors due to limitations in number and size range of supercells included in the extrapolation, but their impacts on the following analysis are marginal.

For better comparison with the experiment, the concentration of defects has been normalized by the total Ti concentration. And μ_O can be represented by the oxygen partial pressure as [43]

$$\mu_O(p,T) = \frac{1}{2}\left[E_{O_2} + kT\left(\ln\frac{pV_Q}{kT} - \ln Z_{rot} - \ln Z_{vib}\right)\right]. \tag{9}$$

Here, E_{O_2} is the total energy of an O_2 molecule, k is the Boltzmann constant, T is the temperature, p is partial pressure of oxygen in sample preparation, $V_Q = (2\pi\hbar^2/mkT)^{\frac{3}{2}}$ is so-called quantum volume, Z_{rot} and Z_{vib} correspond to rotation and vibration partition function [50].

In addition, only the amount of change of μ_O matters that Eq. (9) can be further written as

$$\mu_O = \mu_O(p_0,T) + \tfrac{1}{2}kT\ln(p/p_0) \equiv \mu_O(p_0,T) + \Delta\mu_O. \tag{10}$$

At the reference oxygen partial pressure of $p_0 = 1$ atm, the difference between $\mu_O(p_0,T)$ and $\frac{1}{2}E_{O_2}$ calculated with Eq. (9), which is −1.17, −1.34, −1.51, and −1.69 eV at $T =$ 1673, 1873, 2073, and 2273 K, respectively.

Our calculations on O_2 and single oxygen atom give a 6.03 eV dissociation energy per O_2, similar to a variety of reported calculation values and is known to be overestimated [51]. It has been pointed out in Ref. [51] that such calculated formation energies for metal oxides are systematically overestimated relative to experimental measurements by $\Delta E_{error} \approx 1.36$ eV per O_2, which is equivalent to an underestimation of the formation energy of O_2 of the same amount. This suggests that the chemical potential $\mu_O(p,T)$ in Eq. (9) be underestimated by $\Delta E_{error}/2 \approx 0.68$ eV, and the reference oxygen partial in Eq. (10) and figures in the following need to be revised from p_0 to

$$p_0' = p_0 \exp\left(-\frac{\Delta E_{error}}{kT}\right). \tag{11}$$

In Fig. 2(a), there are mainly six defect species whose concentrations are much higher than other defects in oxygen rich (partial pressure $\sim p_0$, or p_0' considering the correction, the same below) or moderate (partial pressure $\sim 10^{-6} p_0$) conditions. They are the simple defects Ti_{Al}^{0} and Ti_{Al}^{1+}, the ternary $Ti_{Al}\text{-}Ti_{Al}\text{-}V_{Al}$ in $o\text{-}o\text{-}c^{1-}$ configuration which corresponds to the situation that V_{Al}^{3-} locates at c site together with two Ti_{Al}^{1+} occupying o sites, the ternary $V_{Al}^{3-}\text{-}Ti_i^{4+}\text{-}V_{Al}^{3-}$ and $V_{Al}^{3-}\text{-}Al_i^{3+}\text{-}V_{Al}^{3-}$ that contain an interstitial Ti_i^{4+} or Al_i^{3+}, whose nearest two Al neighbors are missing, i.e., become V_{Al}^{3-}, and the quaternary $Ti_{Al}\text{-}Ti_{Al}\text{-}Ti_{Al}\text{-}V_{Al}$ in $o\text{-}o\text{-}o\text{-}c^{0}$ configuration, where three Ti_{Al}^{1+} locate at o sites and V_{Al}^{3-} locates at c site. $o\text{-}o\text{-}o\text{-}c^{0}$ can be viewed as a charge neutral complex formed by the combination between a Ti_{Al}^{1+} and the ternary $o\text{-}o\text{-}c^{1-}$. We notice that none of the complexes among $Ti_{Al}\text{-}Ti_{Al}\text{-}V_{Al}$ in $o\text{-}o\text{-}c^{1-}$, $V_{Al}^{3-}\text{-}Ti_i^{4+}\text{-}V_{Al}^{3-}$, and $V_{Al}^{3-}\text{-}Al_i^{3+}\text{-}V_{Al}^{3-}$ predominate over others as negative charge compensators for Ti_{Al}^{1+} and each of them have a different dependence on fabricating conditions. Thus this should have brought about the rich diversities in properties of different Ti doped samples.

It is noteworthy that the concentration of isolated Ti_{Al}^{0} ions increases gradually as the reductive atmosphere increases to dominate over Ti_{Al}^{1+} ions and their aggregations with V_{Al}^{3-}, while $Ti_{Al}^{0}\text{-}Ti_{Al}^{0}$ and $Ti_{Al}^{0}\text{-}Ti_{Al}^{1+}$ never dominate in the process, even for the high concentration (0.5 at.%) of Ti ions in Ti:Al_2O_3 considered here. In particular, two ternary complexes $V_{Al}^{3-}\text{-}Ti_i^{4+}\text{-}V_{Al}^{3-}$ and $V_{Al}^{3-}\text{-}Al_i^{3+}\text{-}V_{Al}^{3-}$, which contain correspondingly an interstitial ion Ti^{4+} and Al^{3+}, make their presence stable in oxygen rich or moderate situations as a result of strong Coulomb attraction between their compositions. And these two complexes have barely been realized in titanium sapphire before.

The $Ti_{Al}^{1+}\text{-}V_{Al}^{3-}$ defect is the next important negative charge compensator in oxygen rich and moderate conditions, while the concentration of $Ti_{Al}^{0}\text{-}Ti_{Al}^{0}$ first increases rapidly along with Ti_{Al}^{0} as $\Delta\mu_O$ decreases and then approaches a constant at the partial pressure of oxygen of $\sim 10^{-12} p_0$, the typical oxygen poor condition.

Apart from these main defects in Fig. 2(a), Fig. 2(b) illustrates the concentrations of other defects which are relatively minor but still important. We have shown that $Ti_{Al}^{0}\text{-}Ti_{Al}^{0}$ does not contribute to the infrared absorption in the laser operation wavelength ranges centered at ∼800 nm [24], although it might deteriorate laser performance due to excited-states absorption and energy transfer processes. Those defects and complexes composed of only V_{Al}^{3-} and Ti_{Al}^{1+} have a closed shell electronic configuration and are inert to the laser operation in

the visible to near infrared as well. Hence, the minor defects and complexes of the most concern are Ti_{Al}^{0}-Ti_{Al}^{1+} and those complexes containing the Ti_{Al}^{0}-Ti_{Al}^{1+} component, which produces residual infrared absorption [18,24].

As $\Delta\mu_O$ decreases, the concentration of Ti_{Al}^{0}-Ti_{Al}^{1+} first increases and reaches the maximum at around the oxygen moderate condition, then it decreases and finally approaches a constant. It is interesting that Ti_{Al}^{0}-Ti_{Al}^{1+} is very stable and can not be totally eliminated even in an extremely reductive atmosphere. This is caused by the charge neutrality condition in Ti:Al_2O_3 crystal. In a strong reductive atmosphere, most defects are charge neutral but small amounts of Ti_{Al}^{1-} turns up by further reduction of Ti_{Al}^{0}, and Ti_{Al}^{1+} and Ti_{Al}^{0}-Ti_{Al}^{1+} play the positive charge compensators in the crystal.

It has been argued that some V_{Al}^{3-} are localized around the Ti_{Al}^{0}-Ti_{Al}^{1+} pairs based on ESR spectrum [25]. Our calculation supports this observation: there are three multiple complexes which contain Ti_{Al}^{0}-Ti_{Al}^{1+} pair and V_{Al}^{3-}, they are *o*-*o*-*o*-c^{1-}, *o*-*o*-c^{2-}, and *o*-*c*-o^{2-}. The quaternary Ti_{Al}-Ti_{Al}-Ti_{Al}-V_{Al} (*o*-*o*-*o*-c^{1-}) corresponds to V_{Al}^{3-} located at *c* site, two Ti_{Al}^{1+} and one Ti_{Al}^{0} locate at *o* sites. In the ternary complexes *o*-*o*-c^{2-} and *o*-*c*-o^{2-}, the first two sites contain one Ti_{Al}^{0} and one Ti_{Al}^{1+}, while the last site accommodates a V_{Al}^{3-}. Figure 2(b) shows that the concentration of *o*-*o*-*o*-c^{1-} configuration is comparable to that of the Ti_{Al}^{0}-Ti_{Al}^{1+} pair, and dominates at oxygen rich and moderate conditions over the two ternary complexes which contain the Ti_{Al}^{0}-Ti_{Al}^{1+} pair as composition at the rather large total Ti content of 0.5 at.%. Since the defects contain three and two Ti ions scale qualitatively with the cube and square of the content of Ti, respectively, it can be predicted that *o*-*o*-*o*-c^{1-} is less important than Ti_{Al}^{0}-Ti_{Al}^{1+} pairs when the dopant concentration is lower. To sum up, the dominant complex containing Ti_{Al}^{0}-Ti_{Al}^{1+} as component is predicted to be the Ti_{Al}^{0}-Ti_{Al}^{1+} pairs themselves for the cases of moderate to strong reductive condition or samples contain of lower than 0.5 at.% of Ti content. Furthermore, the variation of the concentration of Ti_{Al}^{0}-Ti_{Al}^{1+}, or the residue absorption with reduction atmosphere (represented by oxygen partial pressure) may be carefully measured in experiments to calibrate the systematic error in calculations.

Most V_{Al}^{3-} are combined with other Ti_{Al}^{1+} as complexes, especially when V_{Al}^{3-} locates at the center site of these complexes (see the basic unit in Fig. 1), which greatly reduces the formation energy of the complex by Coulomb interaction between V_{Al}^{3-} and Ti_{Al}^{1+} defects. And of course, the Coulomb interaction between Ti_{Al}^{1+} atoms is the strongest when the V_{Al}^{3-} locates at the center site, which is illustrated also by the binding energies of these complexes (Table I). $(V_{Al}$-Al_i-$V_{Al})^{3-}$, a variant of the simple V_{Al}^{3-} but much more stable than the latter, starts to play the dominant role of negative charge compensator as the reductive atmosphere is approaching the oxygen poor condition. The combination of $(V_{Al}$-Al_i-$V_{Al})^{3-}$ with Ti_{Al}^{1+}'s is potentially stable, but is not expected to be more important than that of V_{Al}^{3-} with Ti_{Al}^{1+}'s. This is due to less-compact geometric arrangements and less favorable Coulomb attractions than a single center V_{Al}^{3-} surrounded by Ti_{Al}^{1+}'s in reducing the formation energy of the complex.

The thermodynamic charge transition levels of the dominant Ti-containing defects and the two most important simple intrinsic defects are illustrated in Fig. 3, and the thermodynamic equilibrium Fermi levels under three reference oxygen partial pressures at 1873 K are also plotted. It is shown that all the negatively-charged defects and complexes contain V_{Al}^{3-} as a composition greatly constrains the upshift of the Fermi level.

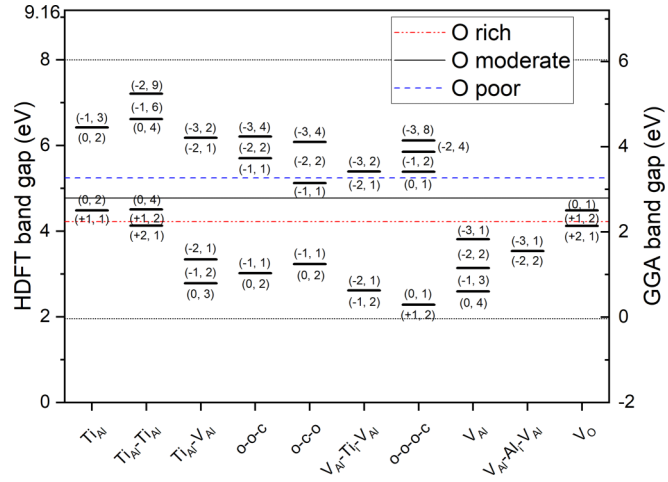

FIG. 3. The defects' thermodynamic transition levels and the Fermi levels at different oxygen partial pressures of p_0 (O rich), $10^{-6}p_0$ (O moderate), and $10^{-12}p_0$ (O poor). The two integers (q, M) are the charge q, and the multiplicity of (near) degenerate ground states, M. We note that all charge transition levels in the band gap are calculated with GGA+U method, the HDFT band gap is obtained via PBE0-type hybrid density functional with HF mixing parameter $\alpha = 0.29$, and the VBM of HDFT is 1.954 eV lower than GGA one according to the alignment of average electron potential in the supercell. Such alignment leads to the estimation of the threshold of Ti^{4+} charge transfer transition $E_{CT}(0) = 4.48$ eV and Ti^{3+} photoionization $E_{PI}(0) = 4.68$ eV, which are correspondingly consistent to the slightly different values of 4.27 and 4.89 eV obtained by our previous PBE0 calculation [24].

In addition, Fig. 4 illustrates how Ti chemical potential and Fermi level depends on the chemical potential of oxygen in Fig. 2. For better understanding, the change of μ_{Ti} is set to relative to the metal (denoted as $\Delta\mu_{Ti}$) and E_F is set to relative to the VBM, i.e., $\Delta\varepsilon_F$. When μ_O decreases, both $\Delta\mu_{Ti}$ and $\Delta\varepsilon_F$ increase. The change of $\Delta\mu_{Ti}$ is smooth and there is a phase transition for the change rate of $\Delta\mu_{Ti}$ when oxygen partial pressure is at around $10^{-6}p_0$, which corresponds to the concentration peak of Ti_{Al}^{0}-Ti_{Al}^{1+} and suggests the charge state change of dominant Ti_{Al} ions. As for $\Delta\varepsilon_F$, it increases rapidly until reaches a limit as μ_O approaches O poor condition where most of defects have been reduced to charge neutrality. Moreover, the change range of E_F is very limited (about 1.2 eV) and localized around the middle of the band gap. It is noted that in the whole range of μ_O considered, the constraint $\Delta\mu_{Ti} \leqslant 0$ is satisfied.

When the crystal is annealing at a lower temperature where the ion mobility is no longer effective, thermodynamic equilibrium between different species can hardly be reached but changes of valence in complexes and defects are possible. At this circumstance, complexes such as *o*-*o*-*c* and *o*-*o*-*o*-*c* are mostly locked correspondingly at *o*-*o*-c^{1-}

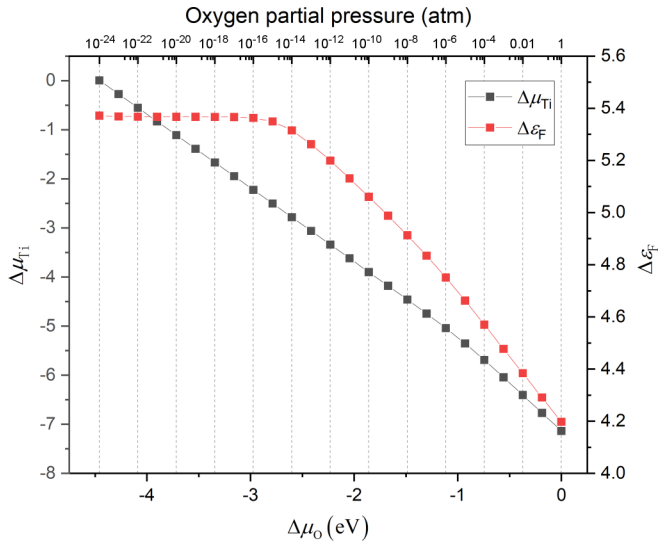

FIG. 4. Dependence of the chemical potential $\Delta\mu_{\mathrm{Ti}}$ relative to Ti metal and the Fermi level $\Delta\varepsilon_F$ relative to VBM of HDFT on the relative oxygen chemical potential $\Delta\mu_{\mathrm{O}}$ and oxygen partial pressure in Fig. 2. The Fermi level relative to VBM of GGA compatible with Table III B is $\Delta\varepsilon'_{\mathrm{F}} = \Delta\varepsilon_{\mathrm{F}} - 1.954$ eV.

($\mathrm{Ti}_{\mathrm{Al}}^{1+}$-$\mathrm{Ti}_{\mathrm{Al}}^{1+}$-$V_{\mathrm{Al}}^{3-}$) and *o-o-o-c*^{0} ($\mathrm{Ti}_{\mathrm{Al}}^{1+}$-$\mathrm{Ti}_{\mathrm{Al}}^{1+}$-$\mathrm{Ti}_{\mathrm{Al}}^{1+}$-$V_{\mathrm{Al}}^{3-}$) valence in oxygen rich and moderate conditions. Although at such valence these complexes do not contain open-shell electrons and do not contribution to the residual infrared absorption, some of them can be converted to lower valence that contain a $\mathrm{Ti}_{\mathrm{Al}}^{0}$-$\mathrm{Ti}_{\mathrm{Al}}^{1+}$ pair as composition and contribute to the residual infrared absorption under more reductive atmosphere. This will counterbalance, to some extent, the influence of converting $\mathrm{Ti}_{\mathrm{Al}}^{0}$-$\mathrm{Ti}_{\mathrm{Al}}^{1+}$ pair to $\mathrm{Ti}_{\mathrm{Al}}^{0}$-$\mathrm{Ti}_{\mathrm{Al}}^{0}$ in the reductive processes. Hence, to obtain high-quality sample, it is essential that those potentially harmful complexes have been significantly eliminated at high-temperature annealing as mentioned in Ref. [28].

To sum up, even at a relatively high Ti doped concentration (0.5 at.%), Fig. 2 shows that the concentration of $\mathrm{Ti}_{\mathrm{Al}}^{0}$-$\mathrm{Ti}_{\mathrm{Al}}^{1+}$ pair is much smaller than (from $\lesssim 10^{-4}$ to $\lesssim 3\times10^{-3}$ of) the total Ti doped concentration. Although the concentration of $\mathrm{Ti}_{\mathrm{Al}}^{0}$-$\mathrm{Ti}_{\mathrm{Al}}^{1+}$ pair is minor, its infrared absorption could be quite strong due to its large oscillator strength compared to the pump absorption of $\mathrm{Ti}_{\mathrm{Al}}^{0}$ [24], and this makes the elimination of the residual infrared absorption very difficult. As illustrated in Fig. 2, when the reductive atmosphere increases, the concentration of $\mathrm{Ti}_{\mathrm{Al}}^{0}$-$\mathrm{Ti}_{\mathrm{Al}}^{1+}$ will increase first and reach the maximum at a moderate reductive condition. The concentration increasing of $\mathrm{Ti}_{\mathrm{Al}}^{0}$-$\mathrm{Ti}_{\mathrm{Al}}^{1+}$ corresponds to the reduction and decomposition of $\mathrm{Ti}_{\mathrm{Al}}^{1+}$ and V_{Al}^{3-} related multiple complexes such like *o-o-o-c*^{0} and *o-o-c*$^{1-}$. Hence, only when these multiple complexes are basically eliminated, the concentration of $\mathrm{Ti}_{\mathrm{Al}}^{0}$-$\mathrm{Ti}_{\mathrm{Al}}^{1+}$ can decrease dramatically. However, further increasing reductive atmosphere to an oxygen extremely poor condition (say, 10^{-18}–10^{-20} atm), which might be impractical or unrealistic due to other unconsidered constraints, will only make a very small influence to reduce the concentration of $\mathrm{Ti}_{\mathrm{Al}}^{0}$-$\mathrm{Ti}_{\mathrm{Al}}^{1+}$. As shown in Fig. 2, the concentration of $\mathrm{Ti}_{\mathrm{Al}}^{0}$-$\mathrm{Ti}_{\mathrm{Al}}^{1+}$ approaches a constant at extremely reductive atmosphere. This phenomenon is caused by the charge neutrality requirement in Ti:Al_2O_3 crystal and the appearance of a small amount of $\mathrm{Ti}_{\mathrm{Al}}^{1-}$ to balance the charge of $\mathrm{Ti}_{\mathrm{Al}}^{1+}$, limiting further reduction of $\mathrm{Ti}_{\mathrm{Al}}^{0}$-$\mathrm{Ti}_{\mathrm{Al}}^{1+}$.

D. Discussions on other defects in Ti:Al_2O_3 crystal

Recently, Ref. [27] proposed Ti_i^{3+}-V_{Al}^{3-} as a new luminous center to illustrate the optical absorption bands at 388 and 460 nm, where V_{Al}^{3-} plays a charge compensator to make Ti_i^{3+} stable [11]. However, based on our calculations, this defect is not stable in that Coulomb interaction attracts Ti_i^{3+} to fill V_{Al}^{3-} and reduces the complex into a simple dopant defect $\mathrm{Ti}_{\mathrm{Al}}^{0}$. A more reasonable candidate is Ti_i^{3+} accompanied by two symmetrically surrounded V_{Al}^{3-}, i.e., (V_{Al}-Ti_i-V_{Al})$^{3-}$ in Table I, which we have shown to be very stable due to the strong Coulomb attractions, despite that the isolated Ti_i^{3+} has a very unfavorable formation energy to exist. It is noted that in both Ti_i^{3+} and (V_{Al}-Ti_i-V_{Al})$^{3-}$, the Ti_i^{3+} dopant ion occupies the centrosymmetric site (point group $S_6 = C_{3i}$) and its optical absorption and emission are predicted to be extremely weak. Regarding the minor optical absorption bands at 388 and 460 nm, a varies of other $\mathrm{Ti}_{\mathrm{Al}}^{0}$-containing complexes are possible contributors, but this is out of our focus here.

Apart from defects and complexes that contain titanium ions, the oxygen vacancy as intrinsic defect in Al_2O_3 bulk, which can capture one or two electron(s) to become F^+ or F center, should also be considered as a potential candidate to illustrate the spectroscopic properties of Ti:Al_2O_3. Actually, Ref. [25] illustrates the 235 and 390 nm excitation bands as the results of F^+ center and F^+ center perturbed by adjacent defects respectively in their reductive-atmosphere annealing samples as ANN$-H2. Reference [52] supposes that there is a superposition of charge transfer band and excitation bands from F or F^+ centers under reductive atmospheres. However, the latest work in Ref. [10] does not support these F center related hypotheses according to their comprehensive spectrum analysis. And according to our calculation of defects concentration (Fig. 2), the contributions of F or F^+ centers only make a presence at the extremely reductive atmosphere.

In addition, the concentrations of positive and negative intrinsic defects are mutually constrained. In specific, $[c(V_{\mathrm{Al}}^{3-})^2\, c(V_{\mathrm{O}}^{2+})^3]^{1/5}$ are related to the per defect formation energy of Schottky quintet as $[2E_f(V_{\mathrm{Al}}^{3-}) + 3E_f(V_{\mathrm{O}}^{2+})]/5 = 4.41$ eV. Since there is a more stable variant V_{Al}^{3-}-Al_i^{3+}-V_{Al}^{3-} to the simple V_{Al}^{3-} with lower formation energy by 1.24 eV, a lower per defect formation energy is obtained for the Schottky quintet as $[2E_f(V_{\mathrm{Al}}^{3-}\text{-}\mathrm{Al}_i^{3+} - V_{\mathrm{Al}}^{3-}) + 3E_f(V_{\mathrm{O}}^{2+})]/5 = 3.92$ eV, in reasonable agreement with the experimental value of 3.83 eV [53].

E. Discussion on the dependence of FOM on concentrations of $\mathrm{Ti}_{\mathrm{Al}}^{0}$ and $\mathrm{Ti}_{\mathrm{Al}}^{1+}$ ions

FOM of Ti:Al_2O_3 laser crystals is defined [10] as the ratio of absorption coefficients between pump band, $\alpha_{\mathrm{Ti}_{\mathrm{Al}}^{0}}$, and residual infrared band, $\alpha_{\mathrm{Ti}_{\mathrm{Al}}^{0}-\mathrm{Ti}_{\mathrm{Al}}^{1+}}$. We have shown that even for a total concentration of Ti ion at 0.5 at%, the upper limit of concern, i.e., the dominant contribution to the residual

infrared should still be from the Ti^0_{Al}-Ti^{1+}_{Al} pairs. In this case, FOM can be further written as

$$\mathrm{FOM} \equiv \frac{\alpha_{Ti^0_{Al}}}{\alpha_{Ti^0_{Al}-Ti^{1+}_{Al}}} = \frac{c_{Ti^0_{Al}}}{c_{Ti^0_{Al}-Ti^{1+}_{Al}}}\frac{f_r}{R}. \tag{12}$$

Here, f_r and R correspond to ratios of oscillator strength and band width of Ti^0_{Al} relative to that of Ti^0_{Al}-Ti^{1+}_{Al} pair, respectively. According to our previous work [24], $f_r \sim 1.0 \times 10^{-3}$, while $R \sim 1/3$ is estimated from experiments [10,28].

It is well-known that annealing the Ti:Al_2O_3 crystal in the reductive atmosphere can reduce the residual infrared absorption [10,25]. Furthermore, Ref. [28] points out that high FOM values can be more favorably obtained for Ti:Al_2O_3 crystals at lower Ti^0_{Al} ions concentration and the annealing process should be carried out at high temperature and carefully controlled. In addition, both the experimental and theoretical analyses from previous works [10,17] find that FOM is inversely proportional to the concentration of isolated Ti^{1+}_{Al} ions which can be illustrated by the Ti^0_{Al}-Ti^{1+}_{Al} pair model.

In this work, we will illustrate that this conclusion is a natural corollary for the Ti^0_{Al}-Ti^{1+}_{Al} pair model, when the defects in Ti:Al_2O_3 crystal reach an thermodynamic equilibrium distribution. And according to our first-principles calculation results, we will give a qualitative explanation for the experimental conclusion in Ref. [28] about improving FOM in Ti:Al_2O_3 laser.

As for defect Ti^0_{Al}, Ti^{1+}_{Al}, and Ti^0_{Al}-Ti^{1+}_{Al} pair, we have the reaction when the Ti:Al_2O_3 reaches its thermodynamical equilibrium

$$Ti^0_{Al} + Ti^{1+}_{Al} \rightleftharpoons Ti^0_{Al}\text{-}Ti^{1+}_{Al}. \tag{13}$$

And the concentrations of these defects satisfy the law of mass action [54] that

$$K_{\mathrm{eq}}(T) = \frac{c_{Ti^0_{Al}}\, c_{Ti^{1+}_{Al}}}{c_{Ti^0_{Al}-Ti^{1+}_{Al}}} = N_r \exp\left(\frac{E_b}{kT}\right). \tag{14}$$

The N_r is a ratio determined by ω and N_{config} of these defects, and E_b is the binding energy of Ti^0_{Al}-Ti^{1+}_{Al} according to Eq. (8). As our calculations show that E_b is almost zero (-0.05 eV and -0.07 eV correspondingly for the nearest and next-nearest Ti^0_{Al}-Ti^{1+}_{Al} pairs), $K_{\mathrm{eq}}(T)$ is only weakly dependent on temperature. At a fixed high-enough annealing temperature T that allows migration of ions, the ratio $c_{Ti^0_{Al}}/c_{Ti^0_{Al}-Ti^{1+}_{Al}}$ is

$$\frac{c_{Ti^0_{Al}}}{c_{Ti^0_{Al}-Ti^{1+}_{Al}}} = \frac{K_{\mathrm{eq}}(T)}{c_{Ti^{1+}_{Al}}}, \tag{15}$$

which is inversely proportional to the concentration of isolated Ti^{1+}_{Al} ions.

Figure 5 plots the $c_{Ti^0_{Al}}/c_{Ti^0_{Al}-Ti^{1+}_{Al}}$ in different annealing conditions. It is compatible with the conclusion in Ref. [28] that the more reductive atmosphere and lower total Ti concentration will lead to the higher FOM. And Eq. (15) provides another insight to understand these observations about improving FOM.

In order to improve FOM, the increase of $K_{\mathrm{eq}}(T)$ and the decrease of Ti^{1+}_{Al} concentration are required. When T and c_{Ti} are fixed, the stronger reductive atmosphere will decrease the Ti^{1+}_{Al} concentration by reducing Ti^{1+}_{Al} to Ti^0_{Al}. And in our calculation, it is found that as the annealing temperature increases, both $K_{\mathrm{eq}}(T)$ and $c_{Ti^{1+}_{Al}}$ increase, and the variation trend of FOM depends on which parameter changes faster. Figure 5(a) shows that, when the oxygen partial pressure is fixed, merely increasing T has no or opposite effect on FOM improvement in oxidation or weak reductive atmosphere, but is effective in medium to strong reductive atmosphere as $c_{Ti^{1+}_{Al}}$ has become relatively small. As for the extremely reductive atmosphere (oxygen partial pressure is less than $10^{-16}p_0$), low annealing temperature will benefit for increasing FOM, however this kind of reductive atmosphere might be hard to realize in experiment. Meanwhile, the oxygen partial pressure needs to

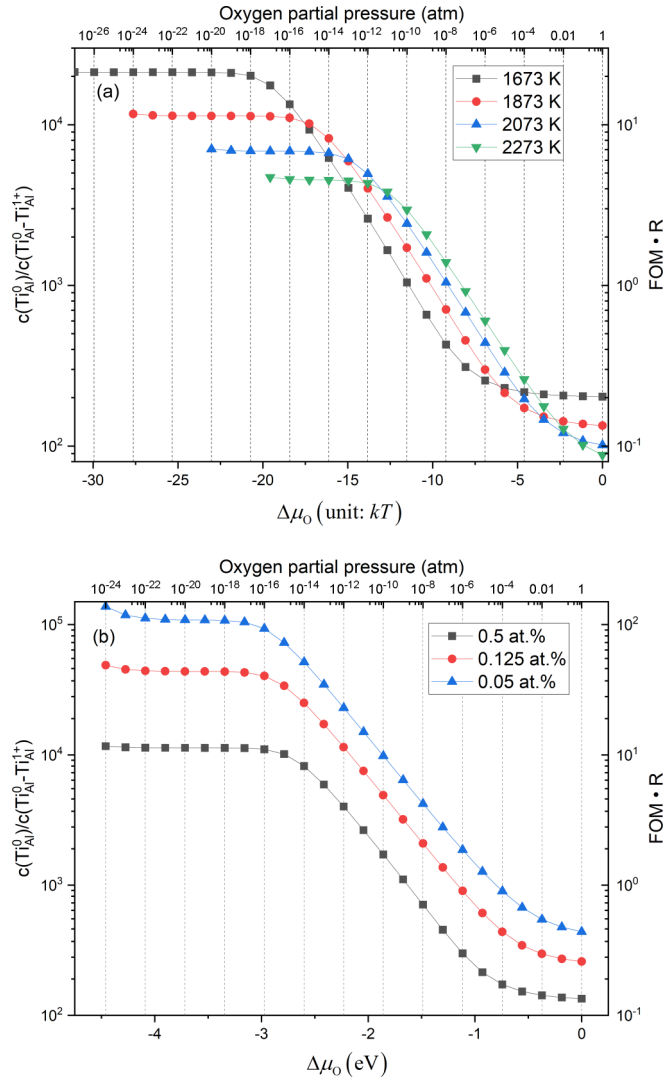

FIG. 5. The $c_{Ti^0_{Al}}/c_{Ti^0_{Al}-Ti^{1+}_{Al}} \sim \mathrm{FOM} \cdot R$ versus the oxygen partial pressure when (a) the total doped Ti concentration is fixed at 0.5 at.% and (b) the annealing temperature is at 1873 K. $R \sim 1/3$ is the radio of effective absorption bandwidth between Ti^0_{Al} and Ti^0_{Al}-Ti^{1+}_{Al} and f_r has been taken as 10^{-3}. It is noted that the unit of $\Delta\mu_O$ in (a) is kT, which equals to 0.1442, 0.1614, 0.1786, and 0.1959 eV for annealing temperature $T = 1673$, 1873, 2073, and 2273 K, respectively. Similar to Fig. 2, Eq.(11) suggests a rescaling of the pressure by the factors 0.80×10^{-4} (1673 K), 2.2×10^{-4} (1873 K), 4.9×10^{-4} (2073 K), and 9.7×10^{-4} (2273 K).

be reduced along with the decrease of annealing temperature in the cooling process as so to maintain or even to increase the favorable strong reductive atmosphere.

Regarding to decreasing c_{Ti}, this is always effective in improving FOM at given annealing temperature T and reductive atmosphere. This is due to the fact that the decrease of the total doped Ti concentration can obviously reduce the concentration of complexes containing two or more $\mathrm{Ti}_{\mathrm{Al}}^{0,1+}$ more effectively than those containing one only. A comparison of three typical concentrations is plotted in Fig. 5(b), which shows that for annealing temperature $T = 1873$ K the FOM can potentially reach ∼36, ∼145, and ∼360 [according to Eq. (16) below] for $c_{\mathrm{Ti}} = 0.5,\ 0.125,\ 0.05$ at.%, respectively. However, a lower c_{Ti} concentration leads to a weaker pump absorption and weaker laser output. Thus there is a tradeoff between increasing FOM and enhancing the absolute strength of output.

When $\mathrm{Ti}_{\mathrm{Al}}^{0}$-$\mathrm{Ti}_{\mathrm{Al}}^{1+}$ pairs are the dominant contribution to the residual infrared absorption and the concentrations of various defect and complexes reach thermodynamical equilibrium distribution at temperature T, FOM can be related to the concentration of Ti^{4+} by Eqs. (12) and (15) as

$$\mathrm{FOM} = \frac{K_{\mathrm{eq}}(T)}{c_{\mathrm{Ti}_{\mathrm{Al}}^{1+}}} \frac{f_r}{R} \simeq \frac{9.3 \times 10^{19}\ \mathrm{cm}^{-3}}{c_{\mathrm{Ti}_{\mathrm{Al}}^{1+}}}. \tag{16}$$

$K_{\mathrm{eq}}(T)$ is only weakly temperature dependent, and $T = 1873$ K, $f_r \sim 10^{-3}$, $R \sim 1/3$ are adopted to obtain the simple numerical expression at the right hand side of Eq. (16) that serves as a reference for analyzing experimental data.

Based on Eq. (16), the series of samples labeled SY2a,d ($c_{\mathrm{Ti}_{\mathrm{Al}}^{1+}} = 2.83 \times 10^{17}\ \mathrm{cm}^{-3}$, $\mathrm{FOM}_{\mathrm{calc}} = 329$, $\mathrm{FOM}_{\mathrm{expt}} = 331$), CT2a ($10.4 \times 10^{17}$, 90, 89), SY7b ($11.4 \times 10^{17}$, 82, 86), and CT1a ($22.1 \times 10^{17}$, 42, 31) from Table 12 of Ref. [10] have roughly reached the theoretically limit at the given Ti^{4+} content, while the substantial smaller measured FOMs than predicted by Eq. (16) in some other samples indicate that appropriate further annealing might improve the FOMs of these samples for the given Ti^{4+} content. More details can be founded in Sec. S5 [41].

In addition, Ref. [10] also reported that a square-law dependence of the residual infrared absorption on $\mathrm{Ti}_{\mathrm{Al}}^{0}$ concentration is observed in a series of Synoptics-label samples and argued that some of the residual infrared absorption might not due to $\mathrm{Ti}_{\mathrm{Al}}^{0}$-$\mathrm{Ti}_{\mathrm{Al}}^{1+}$ pairs. Reference [17] took the case of given T and μ_{O} as an example to illustrate that this square-law dependence does not contradict the pair model for residual infrared absorption. It is supposed that the relationship $c_{\mathrm{Ti}_{\mathrm{Al}}^{0}-\mathrm{Ti}_{\mathrm{Al}}^{1+}} = \kappa c_{\mathrm{Ti}_{\mathrm{Al}}^{0}}^{2}$ holds for given T and the coefficient κ only depends weakly on temperature. Here we use Eq. (15) to give a more comprehensive illustration that

$$\frac{c_{\mathrm{Ti}_{\mathrm{Al}}^{0}-\mathrm{Ti}_{\mathrm{Al}}^{1+}}}{c_{\mathrm{Ti}_{\mathrm{Al}}^{0}}^{2}} = \frac{c_{\mathrm{Ti}_{\mathrm{Al}}^{1+}}}{c_{\mathrm{Ti}_{\mathrm{Al}}^{0}}} \cdot \frac{1}{K_{\mathrm{eq}}(T)} = e^{\frac{E_F^0 - E_F}{kT}} K_{\mathrm{eq}}(T)^{-1}. \tag{17}$$

Here $E_F^0 = \varepsilon(\mathrm{Ti}_{\mathrm{Al}}, +1/0)$ is thermodynamic charge transition level of $\mathrm{Ti}_{\mathrm{Al}}^{q}$ ($q = 0, +1$), i.e., the Fermi level where the formation energies of $\mathrm{Ti}_{\mathrm{Al}}^{0}$ and $\mathrm{Ti}_{\mathrm{Al}}^{1+}$ equal, while the actual Fermi level E_F relies on the content of various defects in the Ti:Al_2O_3 crystal, which is determined by the charge neutrality condition in Eq. (5). There might not be a simple expression to relate E_F to the annealing temperature T, the total doped concentration c_{Ti} and the relative reductive atmosphere μ_{O}. However, our calculations show that E_F increases slightly with increasing temperature by a much small amount than the increase of $k_B T$, and decreases slightly with the increase of μ_{O} and c_{Ti}.

Thus, if the relationship $c_{\mathrm{Ti}_{\mathrm{Al}}^{0}-\mathrm{Ti}_{\mathrm{Al}}^{1+}} = \kappa c_{\mathrm{Ti}_{\mathrm{Al}}^{0}}^{2}$ is satisfied, E_F needs to be only dependent weakly on the above-mentioned independent variables. In Ref. [10], the series Synoptics-label samples, which is observed to obey this square law, is grown and annealed in the same atmospheric condition. It can be regarded as the situation that both the T and μ_{O} are fixed while the total Ti concentration is varied. Although E_F does change when c_{Ti} decreases from 0.5 at.% to 0.05 at.%, the variation of E_F is so small that the zero-origin parabola behavior of $c_{\mathrm{Ti}_{\mathrm{Al}}^{0}-\mathrm{Ti}_{\mathrm{Al}}^{1+}} = \kappa c_{\mathrm{Ti}_{\mathrm{Al}}^{0}}^{2}$ holds, which is also observed in our calculation, consistent with previous calculation [17]. This shows that the correlation between residual infrared absorption with the square of Ti^{3+} concentration is not a definite departure from the $\mathrm{Ti}_{\mathrm{Al}}^{0}$-$\mathrm{Ti}_{\mathrm{Al}}^{1+}$ model for the residual infrared absorption.

IV. CONCLUSION

We obtained formation energies and binding energies of potentially significant defects and complexes, and reveal two new potentially significant negatively charged complexes, $(V_{\mathrm{Al}}\text{-}\mathrm{Al}_i\text{-}V_{\mathrm{Al}})^{3-}$ and $(V_{\mathrm{Al}}\text{-}\mathrm{Ti}_i\text{-}V_{\mathrm{Al}})^{2-}$, i.e., interstitial Al^{3+} and Ti^{4+} surrounded by two surrounding aluminium vacancies V_{Al}^{3-}. Based on these results we simulated the variation of their concentrations under different processing temperature and reductive atmosphere, and revealed the mechanism why the residual infrared absorption, which is related to $\mathrm{Ti}_{\mathrm{Al}}^{0}$-$\mathrm{Ti}_{\mathrm{Al}}^{1+}$ pair, is so difficult to eliminate in Ti:Al_2O_3 laser crystal.

V_{Al}^{3-} [including its more stable and balanced variant $(V_{\mathrm{Al}}\text{-}\mathrm{Al}_i\text{-}V_{\mathrm{Al}})^{3-}$] plays a significant role from weak to moderate reductive atmospheres and even beyond: V_{Al}^{3-} are combined with other $\mathrm{Ti}_{\mathrm{Al}}^{1+}$ as complexes, especially when V_{Al}^{3-} locates at the center site of these complexes (see the basic unit in Fig. 1), which greatly reduces the formation energy of the complex by Coulomb interaction between V_{Al}^{3-} and $\mathrm{Ti}_{\mathrm{Al}}^{1+}$ defects; $(V_{\mathrm{Al}}\text{-}\mathrm{Al}_i\text{-}V_{\mathrm{Al}})^{3-}$, a variant of the simple V_{Al}^{3-} but being much more stable, starts to play the dominant role of negative charge compensator as the reductive atmosphere is approaching the oxygen poor condition. When the reductive atmosphere increases, those V_{Al}^{3-} and $\mathrm{Ti}_{\mathrm{Al}}^{1+}$ related complexes will decompose and some of them will be transformed to $\mathrm{Ti}_{\mathrm{Al}}^{0}$-$\mathrm{Ti}_{\mathrm{Al}}^{1+}$. In addition, if the annealing process is insufficient or the annealing temperature is not high enough that the movement of defects is restricted but electron hopping remains, complexes containing V_{Al}^{3-} and two or more $\mathrm{Ti}_{\mathrm{Al}}^{1+}$ can still be reduced to complexes containing $\mathrm{Ti}_{\mathrm{Al}}^{0}$-$\mathrm{Ti}_{\mathrm{Al}}^{1+}$. Furthermore, although V_{Al}^{3-} related complexes can be eliminated in a strong reductive atmosphere, $\mathrm{Ti}_{\mathrm{Al}}^{1+}$ and $\mathrm{Ti}_{\mathrm{Al}}^{0}$-$\mathrm{Ti}_{\mathrm{Al}}^{1+}$ still exist to compensate $\mathrm{Ti}_{\mathrm{Al}}^{1-}$, which replaces V_{Al}^{3-} related complexes to act the role as negative charge defect.

The expression of the figure of merit (FOM) for Ti:Al_2O_3 laser crystals, i.e., the ratio of absorption coefficients between pump band and residual infrared band, is obtained in terms of

the concentrations of Ti^{0}_{Al} and Ti^{0}_{Al}-Ti^{1+}_{Al}. Then we obtained and discussed the variation of FOM with reductive atmosphere for a variety of annealing temperatures or total titanium dopant concentrations under the assumption of thermodynamical equilibrium distribution of defects. In particular, a simple expression is obtained to relate the achievable FOM to the inverse of Ti^{1+}_{Al} concentration, and serves as a reference for analyzing experimental results.

Based on our simulations presented in Secs. III C and III E, we propose the following two potentially effective methods to eliminate the residual infrared absorption.

Firstly, as Ref. [28] has already mentioned, enhancing the reductive atmosphere, i.e., decreasing oxygen partial pressure at elevated temperatures, benefits the elimination of Ti^{0}_{Al}-Ti^{1+}_{Al} related pairs. In addition, as is illustrated in Fig. 5(a), by reducing the oxygen partial pressure so as to keep or even to increase the strong reductive atmosphere when the annealing temperature decreases is beneficial.

Secondly, V^{3-}_{Al} is the key player in decreasing the formation energies of complexes containing V^{3-}_{Al} and Ti^{1+}_{Al}, and in acting as charge compensators for positively charged dopants and complexes. At weak to moderate reductive atmospheres, it is one of the key issues to decompose the complexes formed by aggregation of one or more Ti ions with V^{3-}_{Al}, or to decrease the total concentration of V^{3-}_{Al} [including its variant $(V_{Al}\text{-}Al_i\text{-}V_{Al})^{3-}$] altogether. We propose the Al ion injection or annealing in Al vapor mentioned in Ref. [26] as a prospective method to eliminate essentially the effect of V^{3-}_{Al}. This method could potentially introduce other defects like Al interstitial, and so further annealing in suitable reductive atmosphere and temperatures would be required.

Finally, in strong and extremely reductive atmosphere, isolated Ti substitution is dominant over intrinsic defects of Al_2O_3 that a tiny amount of Ti^{0}_{Al} will further reduce to Ti^{1-}_{Al} to balance the charge of Ti^{1+}_{Al}, limiting further reduction of Ti^{0}_{Al}-Ti^{1+}_{Al}, but this effect can be reduced by additional lower temperature reductive-atmosphere annealing, which will further reduce some Ti^{1+}_{Al} to Ti^{0}_{Al} and Ti^{0}_{Al}-Ti^{1+}_{Al} to Ti^{0}_{Al}-Ti^{0}_{Al}.

These formation energies for simple defects and the binding energies for complexes obtained in this work may serve as the basis for simulations and design various quenching and annealing processes to reduce harmful defect species by taking temperature-dependent ion diffusion rates into account. Furthermore, the data may need to be supplemented with additional calculations for other potential defects or complexes and revised with improved Gibbs formation energies. The impact of the interesting $(V_{Al}\text{-}Al_i\text{-}V_{Al})^{3-}$ complex as a stable variant of V^{3-}_{Al} on the properties of pristine α-Al_2O_3 crystals may require further attentions.

ACKNOWLEDGMENTS

The numerical calculations in this paper were partially performed on the supercomputing system in the Supercomputing Center of University of Science and Technology of China. This work was financially supported by the National Key Research and Development Program of China (Grants No. 2018YFA0306600 and No. 2016YFB0701001) and the National Natural Science Foundation of China (Grants No. 11974338, No. 61635012, and No. 11874275).

[1] P. F. Moulton, J. Opt. Soc. Am. B **3**, 125 (1986).
[2] A. Sanchez, R. E. Fahey, A. J. Strauss, and R. L. Aggarwal, Opt. Lett. **11**, 363 (1986).
[3] H. Kiriyama, A. S. Pirozhkov, M. Nishiuchi, Y. Fukuda, K. Ogura, A. Sagisaka, Y. Miyasaka, M. Mori, H. Sakaki, N. P. Dover, K. Kondo, J. K. Koga, T. Z. Esirkepov, M. Kando, and K. Kondo, Opt. Lett. **43**, 2595 (2018).
[4] W. Li, Z. Gan, L. Yu, C. Wang, Y. Liu, Z. Guo, L. Xu, M. Xu, Y. Hang, Y. Xu, J. Wang, P. Huang, H. Cao, B. Yao, X. Zhang, L. Chen, Y. Tang, S. Li, X. Liu, S. Li *et al.*, Opt. Lett. **43**, 5681 (2018).
[5] P. F. Moulton, J. G. Cederberg, K. T. Stevens, G. Foundos, M. Koselja, and J. Preclikova, Opt. Mater. Express **9**, 2131 (2019).
[6] F. Tang, B. Shi, Q. Zhang, C. Zhou, Y. Bu, and J. Li, Laser Phys. **30**, 125802 (2020).
[7] D. S. McClure, J. Chem. Phys. **36**, 2757 (1962).
[8] B. F. Gächter and J. A. Koningstein, J. Chem. Phys. **60**, 2003 (1974).
[9] R. C. Powell, J. L. Caslavsky, Z. AlShaieb, and J. M. Bowen, J. Appl. Phys. **58**, 2331 (1985).
[10] P. F. Moulton, J. G. Cederberg, K. T. Stevens, G. Foundos, M. Koselja, and J. Preclikova, Opt. Mater. Express **9**, 2216 (2019).
[11] K. Matsunaga, A. Nakamura, T. Yamamoto, and Y. Ikuhara, Phys. Rev. B **68**, 214102 (2003).
[12] J. K. Bristow, D. Tiana, S. C. Parker, and A. Walsh, J. Mater. Chem. A **2**, 6198 (2014).
[13] L. Y. Kravchenko and D. V. Fil, J. Appl. Phys. **123**, 023104 (2018).
[14] T. Biswas and M. Jain, Phys. Rev. B **99**, 144102 (2019).
[15] X.-K. Hu, B. Wu, Y. Yang, Y. Yeung, C.-G. Ma, and M. Brik, J. Alloys Compd. **847**, 156459 (2020).
[16] T. Futazuka, R. Ishikawa, N. Shibata, and Y. Ikuhara, Phys. Rev. Materials **4**, 073602 (2020).
[17] L. Y. Kravchenko and D. V. Fil, Phys. Rev. Research **2**, 023135 (2020).
[18] R. L. Aggarwal, A. Sanchez, M. M. Stuppi, R. E. Fahey, A. J. Strauss, W. R. Rapoport, and C. P. Khattak, IEEE J. Quantum Electron. **24**, 1003 (1988).
[19] W. Kohn and L. J. Sham, Phys. Rev. **140**, A1133 (1965).
[20] C. Lee, W. Yang, and R. G. Parr, Phys. Rev. B **37**, 785 (1988).
[21] A. D. Becke, J. Chem. Phys. **98**, 1372 (1993).
[22] J. P. Perdew, K. Burke, and M. Ernzerhof, Phys. Rev. Lett. **77**, 3865 (1996).
[23] K. Matsunaga, T. Mizoguchi, A. Nakamura, T. Yamamoto, and Y. Ikuhara, Appl. Phys. Lett. **84**, 4795 (2004).
[24] W. Jing, M. Liu, J. Wen, L. Ning, M. Yin, and C.-K. Duan, Phys. Rev. B **104**, 165103 (2021).

[25] M. Yamaga, T. Yosida, S. Hara, N. Kodama, and B. Henderson, J. Appl. Phys. **75**, 1111 (1994).
[26] P. Fielitz, S. Ganschow, K. Kelm, and G. Borchardt, Acta Mater. **195**, 416 (2020).
[27] X. Han, X. Feng, W. Li, and S. Guo, Opt. Mater. (Amsterdam) **105**, 109881 (2020).
[28] J. F. Pinto, L. Esterowitz, G. H. Rosenblatt, M. Kokta, and D. Peressini, IEEE J. Quantum Electron. **30**, 2612 (1994).
[29] G. Kresse and J. Hafner, Phys. Rev. B **47**, 558 (1993).
[30] G. Kresse and J. Hafner, Phys. Rev. B **49**, 14251 (1994).
[31] G. Kresse and J. Furthmüller, Phys. Rev. B **54**, 11169 (1996).
[32] G. Kresse and J. Furthmüller, Comput. Mater. Sci. **6**, 15 (1996).
[33] P. E. Blöchl, Phys. Rev. B **50**, 17953 (1994).
[34] G. Kresse and D. Joubert, Phys. Rev. B **59**, 1758 (1999).
[35] J. P. Perdew, A. Ruzsinszky, G. I. Csonka, O. A. Vydrov, G. E. Scuseria, L. A. Constantin, X. Zhou, and K. Burke, Phys. Rev. Lett. **100**, 136406 (2008).
[36] Y. Hinuma, H. Hayashi, Y. Kumagai, I. Tanaka, and F. Oba, Phys. Rev. B **96**, 094102 (2017).
[37] V. I. Anisimov, J. Zaanen, and O. K. Andersen, Phys. Rev. B **44**, 943 (1991).
[38] S. L. Dudarev, G. A. Botton, S. Y. Savrasov, C. J. Humphreys, and A. P. Sutton, Phys. Rev. B **57**, 1505 (1998).
[39] S. Lany and A. Zunger, Phys. Rev. B **80**, 085202 (2009).
[40] P. Deák, Q. Duy Ho, F. Seemann, B. Aradi, M. Lorke, and T. Frauenheim, Phys. Rev. B **95**, 075208 (2017).
[41] See Supplemental Material at http://link.aps.org/supplemental/10.1103/PhysRevB.104.165104 for the detail of the influence of Gamma point integration to defect formation energy; the influence of lattice distortion for charged defect clusters in our calculations; the energy barrier between Ti (or Al) interstitial and Al vacancy; formation energy diagram for important defects and complexes in our maniscript, which shows the relationship between formation energy and Fermi level in different synthesis conditions; the comparison of theoretical FOM with observation results.
[42] C. G. Van de Walle and J. Neugebauer, J. Appl. Phys. **95**, 3851 (2004).
[43] C. Freysoldt, B. Grabowski, T. Hickel, J. Neugebauer, G. Kresse, A. Janotti, and C. G. Van de Walle, Rev. Mod. Phys. **86**, 253 (2014).
[44] T. R. Durrant, S. T. Murphy, M. B. Watkins, and A. L. Shluger, J. Chem. Phys. **149**, 024103 (2018).
[45] C. W. M. Castleton, A. Höglund, and S. Mirbt, Phys. Rev. B **73**, 035215 (2006).
[46] A. Goyal, P. Gorai, H. Peng, S. Lany, and V. Stevanović, Comput. Mater. Sci. **130**, 1 (2017).
[47] W. Jing, ab-crystal-library, (2019), GitHub repository, https//github.com/jingslaw/ab-crystal-library.
[48] M. S. Dresselhaus, G. Dresselhaus, and A. Jorio, *Group Theory: Application to the Physics of Condensed Matter* (Springer Science & Business Media, Heidelberg, 2007).
[49] I. T. McKinnie, A. L. Oien, D. M. Wanington, P. N. Tonga, L. A. W. Gloster, and T. A. King, IEEE J. Quantum Electron. **33**, 1221 (1997).
[50] T. L. Hill, *An Introduction to Statistical Thermodynamics* (Addison-Wesley, Boston, 1960), p. 153.
[51] L. Wang, T. Maxisch, and G. Ceder, Phys. Rev. B **73**, 195107 (2006).
[52] V. B. Mikhailik, H. Kraus, D. Wahl, and M. S. Mykhaylyk, Appl. Phys. Lett. **86**, 101909 (2005).
[53] S. K. Mohapatra and F. A. Kröger, J. Am. Ceram. Soc. **61**, 106 (1978).
[54] J. P. Sethna, *Statistical Mechanics: Entropy, Order Parameters, and Complexity* (Oxford University Press, Oxford, 2006).